Available online at www.sciencedirect.com
SCIENCE DIRECT®
Journal of Nuclear Materials 344 (2005) 94–99
journal of nuclear materials
www.elsevier.com/locate/jnucmat

A miscibility gap in $LiF–BeF_2$ and $LiF–BeF_2–ThF_4$

J.P.M. van der Meer [a,*], R.J.M. Konings [a], M.H.G. Jacobs [b], H.A.J. Oonk [b]

[a] European Commission, Joint Research Centre, Institute for Transuranium Elements, P.O. Box 2340, 76125 Karlsruhe, Germany
[b] Petrology Group, Utrecht University, Budapestlaan 4, 3584 CD Utrecht, The Netherlands

Abstract

$LiF–BeF_2$ and $LiF–BeF_2–ThF_4$ are key systems for Molten Salt Reactor fuel. The liquid phase of these systems has been assessed using Redlich–Kister polynomials. The result shows a miscibility gap on the BeF_2-rich side. This has never been proven experimentally. Nevertheless, evidence for a two liquids region is given by the fact that such a region exists in the analogous $MgO–SiO_2$ system. Also the ternary system $LiF–BeF_2–ZrF_4$ contains such a miscibility gap in the BeF_2 corner.

1. Introduction

The Generation IV programme comprises six future reactor systems. One of them is the Molten Salt Reactor. The concept of this reactor, in which the fuel is dissolved in a circulating molten fluoride salt mixture, was already developed in the 1960s in Oak Ridge National Laboratory, USA. One purpose of the reactor was the breeding of uranium from thorium. Neutron capture of ^{232}Th forms ^{233}Pa, which decays to ^{233}U, a fissile isotope. To obtain an optimum neutron balance and also to meet other important thermal and physicochemical demands, a composition of mainly $LiF–BeF_2$ has proved to be the most viable matrix for the fuel to dissolve in. So in this context, the systems $LiF–BeF_2$ and $LiF–BeF_2–ThF_4$ are of major importance.

$LiF–BeF_2$ was also considered as a 'weakened' analogue for $MgO–SiO_2$ and $ZnO–SiO_2$ by Goldschmidt (for example in [1,2]), because the size of the fluor ion (13.6 pm) and of the oxygen ion (14.0 pm) are nearly similar and the charge is reduced from −2 to −1. Since melting temperatures for the fluorides are significantly lower than for the silicates, thermal and calorimetric investigation of the former was technically easier to perform, particularly in the past.

For these reasons, the $LiF–BeF_2$ phase diagram has been investigated by several researchers, for example Thilo and Lehmann [1], Roy et al. [3,4], Novoselova et al. [5], Thoma et al. [6] and Romberger et al. [7]. However, disagreements exist between the results, especially on the BeF_2-rich side, probably because of the experimental difficulties to perform measurements on the highly viscous melt. Molten BeF_2 is, as SiO_2, known to form glass easily. Glass-formation in a melt results inevitably in supercooling effects during thermal analysis.

Regarding the Molten Salt Reactor concept in Generation IV, no fixed fuel composition is existing yet. Several salt compositions have been proposed for MSR fuel, depending on the exact use and design of the system.

* Corresponding author.
E-mail address: juliette.vandermeer@itu.fzk.de (J.P.M. van der Meer).

0022-3115/$ - see front matter © 2005 Elsevier B.V. All rights reserved.
doi:10.1016/j.jnucmat.2005.04.023

Numerous relevant phase diagrams have been investigated in the past, but it is likely that compositions, different from the ones for which the phase diagrams are presently known, will be used in the future. For the evaluation of melting temperatures of fuel salt compositions in multicomponent systems with LiF, BeF_2, but also NaF and/or RbF as solvent members, we are developing a thermodynamic database. In this framework, the LiF–BeF_2 system and the ternary system of LiF–BeF_2–ThF_4 have been assessed, using the CALPHAD method.

2. Method

Gibbs energy functions of all phases of the system and especially the excess Gibbs energy coefficients of the solution phases are necessary to calculate a T–X phase diagram. When they are unknown, which is rather the rule than exception, they can be obtained by performing a thermodynamic assessment. This is done by making use of the known Gibbs energy functions of the compounds and the available experimental data in the following way: The Gibbs energy functions for the relevant compounds are set up after careful investigation of thermodynamic tables [8] in such a way that they are described as the polynomial in Eq. (1)

$$G(T) = a + bT + cT\ln(T) + \sum d_i T^i. \tag{1}$$

For each phase, Gibbs energy functions have been defined. The Gibbs energy is derived from the temperature dependence of enthalpy and entropy, which in turn are dependent on $C_p(T)$ (Eqs. (2) and (3)). By convention, the reference state for the enthalpy H_{ref} equals the enthalpy of formation from the elements at $T = 298.15$ K and $p = 1$ bar. S^0 (298.15) is used as a reference state for the entropy at $T = 298.15$ K and $p = 1$ bar, but it should be kept in mind that the third law holds for the entropy, i.e. it is zero at 0 K

$$H(T) = H_{\mathrm{ref}} + \int_{T_{\mathrm{ref}}}^{T} C_p \,\mathrm{d}T, \tag{2}$$

$$S(T) = \int_{T=0}^{T} \frac{C_p}{T}\,\mathrm{d}T, \tag{3}$$

$$S(T) = S^0(298.15) + \int_{T_{\mathrm{ref}}}^{T} \frac{C_p}{T}\,\mathrm{d}T. \tag{4}$$

The Gibbs energy is then obtained from the Gibbs–Helmholtz equation (Eq. (5))

$$G(T) = H(T) - S(T)T. \tag{5}$$

Redlich–Kister polynomials are used to describe the excess parameters and are defined as in Eq. (6) for binary systems

$$\Delta_{xs}G = X_A X_B \sum_{k=0}^{N} {}^{k}L_{A,B}(X_A - X_B)^k, \tag{6}$$

${}^{k}L_{A,B}$ are the interaction coefficients, of which the temperature dependence is defined in the same way as Eq. (2). However, in most cases a simple linear dependence is sufficient (Eq. (7)):

$${}^{k}L_{A,B} = {}^{k}p_{A,B} + {}^{k}q_{A,B}T. \tag{7}$$

The coefficients ${}^{k}p_{A,B}$ and ${}^{k}q_{A,B}$ were optimized for the three different binary systems A–B, namely LiF–ThF_4, LiF–BeF_2 and BeF_2–ThF_4. For this purpose, the optimization module of FactSage 5.3 [9] was used, which makes use of the Bayesian optimization algorithm. This is a genetic algorithm, based on the estimation of a probability distribution function. A given experimental data set and initial estimates are used to generate new candidate solutions [10] in such a way that an optimum fit between the Gibbs energy functions and the experimental values is obtained. The system LiF–BeF_2 has also been assessed using the BINGSS program [11] that makes use of the least square method to get a best fit between the experimental data and optimized Gibbs energy coefficients.

3. Results and discussion

3.1. The binary phase diagrams

The Gibbs energy functions of the pure compounds LiF, BeF_2, ThF_4 and of the intermediate compound Li_2BeF_4 were derived from thermodynamic tables. Thermodynamic functions of the intermediate compounds in the LiF–ThF_4 system were not known and were obtained by optimization in FactSage 5.3. Table 1 contains the Gibbs energy functions used in this work.

The excess coefficients needed for the liquid phase in order to describe the phase diagrams of LiF–BeF_2, LiF–ThF_4 and BeF_2–ThF_4 in a satisfying way are listed in Table 2. It must be noted that, though p can be considered as an enthalpy term and q as an entropy term, these coefficients here are essentially mathematical, because of the lack of calorimetric experimental data.

Figs. 1–3 show the assessed phase diagrams of LiF–BeF_2, LiF–ThF_4 and BeF_2–ThF_4 together with the known experimental data.

The calculated phase diagram of the LiF–BeF_2 system in Fig. 1 reproduces the diagram that is proposed on the basis of the experimental results, as for example by Thoma et al. [6], but for one exception. The calculated diagram shows a miscibility gap in the BeF_2-rich side. Assessments using FactSage and BINGSS gave comparable results. There was no other way to perform a successful parameter optimization than to allow a miscibility gap in the liquid phase, in order to let the entropy of fusion of BeF_2 be in concordance with the experimental liquidus data. The entropy of fusion of

Table 1
$\Delta_f H^0(298.15)$ (kJ mol^{-1}), $S^0(298.15)$ (J K^{-1} mol^{-1}) and C_p data for the pure components and intermediate compounds of the system LiF–BeF_2–ThF_4

Comp.	$\Delta_f H^0(298.15)$	$S^0(298.15)$	a	bT	cT^{-2}
LiF(l)[a]	−599.931	43.085	64.219		
BeF_2(l)[a]	−1021.658	60.495	40.984	4.4936E−02	
ThF_4(l)[a]	−2064.491	156.629	133.900		
LiF(cr)[a]	−616.931	35.660	43.051	1.7322E−02	−5.6853E+05
BeF_2(cr, α)[a,b]	−1026.800	53.354	19.181	1.0954E−01	
BeF_2(cr, β)[a,b]	−1025.560	56.114	39.457	4.6255E−02	
ThF_4(cr)[a]	−2097.900	142.050	122.173	8.3700E−03	−1.2550E+06
$2LiF\cdot BeF_2$(cr)[c]	−2274.254	129.483	90.779	1.4915E−01	1.9708E+05
$3LiF\cdot ThF_4$(cr)[d]	−4031.051	184.164	251.327	6.0335E−02	−2.9606E+06
$LiF\cdot ThF_4$(cr)[d]	−2812.701	88.713	165.224	2.5692E−02	−1.8235E+06
$LiF\cdot 2ThF_4$(cr)[d]	−4916.685	241.627	287.397	3.4662E−02	−3.0785E+06
$LiF\cdot 4ThF_4$(cr)[d]	−9155.485	494.702	531.743	5.0802E−02	−5.5885E+06

[a] Data taken from an internal report [22].
[b] A transition occurs at 500 K in solid BeF_2, where the crystal structure changes from low quartz to high quartz.
[c] Data from NIST-JANAF thermochemical tables [8]. An extra term in the C_p function: $-1.8416E{-}08T^2$.
[d] Obtained by optimization.

Table 2
Optimized ${}^k p_{A,B}$ and ${}^k q_{A,B}$ of the liquid phase for LiF–BeF_2, LiF–ThF_4 and BeF_2–ThF_4

A, B	k	${}^k p_{A,B}$/J mol^{-1}	${}^k q_{A,B}$/J K^{-1} mol^{-1}
LiF–BeF_2	0	−15580	−11.645
	1	71320	−63.487
	2	4805.8	0.000
LiF–ThF_4	0	−14369	106.09
	1	56028	−43.643
BeF_2–ThF_4	0	5431.9	−0.3181
	1	6339.2	−8.3035

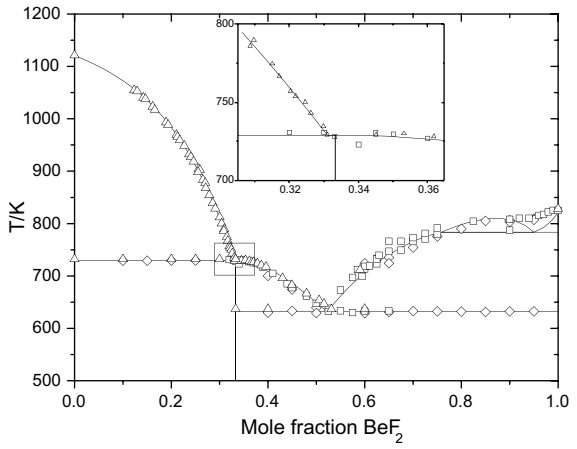

Fig. 1. The assessed LiF–BeF_2 diagram, with an enlargement of the area around the congruently melting Li_2BeF_4: (◇) experimental data by Roy et al. [4]; (□) data by Thoma et al. [6] and (△) data by Romberger et al. [7].

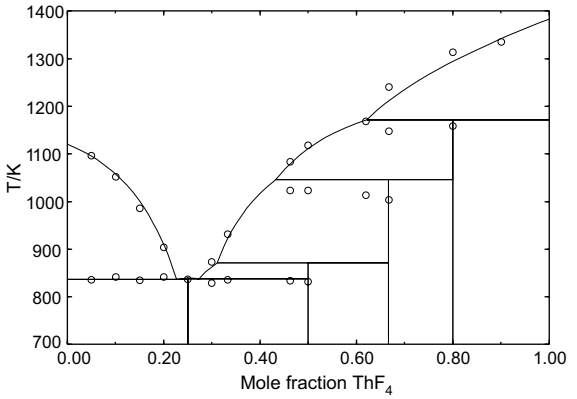

Fig. 2. The assessed LiF–ThF_4 diagram: (○) experimental data from Thoma et al. [17].

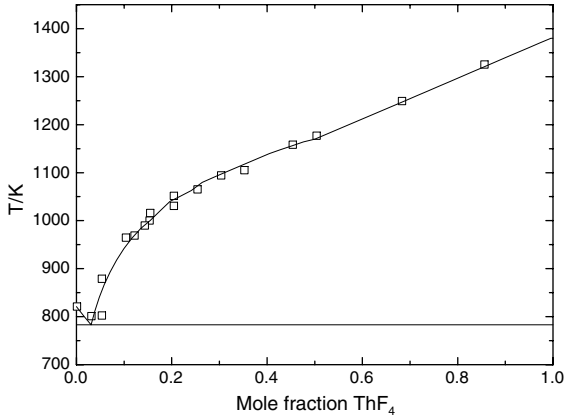

Fig. 3. The assessed BeF_2–ThF_4 diagram: (□) experimental data from Thoma et al. [19].

the bounding component defines the initial slope of the liquidus curve at that component in a T–X diagram [12]

$$\frac{dT}{dX} = \frac{RT_{fus}}{\Delta_{fus}S^0}. \quad (8)$$

The initial slope at $X = BeF_2$ proposed by Thoma et al. suggests $\Delta_{fus}S^0 \simeq 17\ J\ K^{-1}\ mol^{-1}$ or $\Delta_{fus}H^0 \simeq 13.7$ kJ mol^{-1}. The experimental value is considerably lower, $\Delta_{fus}S^0 \simeq 5.4\ J\ K^{-1}\ mol^{-1}$ and $\Delta_{fus}H^0 \simeq 4.5$ kJ mol^{-1} and is well-established. Also Vallet and Braunstein [13] calculated a miscibility gap in the LiF–BeF_2 system. They used the Cook–Hilliard method [14] to compute the binodal and spinodal curves. For this method, liquidus data and extrapolated data on isothermal activity coefficients were needed, which were provided by several phase diagram measurements [6,7] and an electromotive force study [15]. The result was a two-liquid region, which is almost entirely below the liquidus, i.e. metastable, except for a small section around the critical temperature of $T_c = 807$ K at 0.781 mole fraction. The shape of the miscibility gap is slightly different from the one calculated in our assessment process.

A miscibility gap in LiF–BeF_2 is also in concordance with the analogous MgO–SiO_2 system, which has a significant gap at the SiO_2-rich side, between 0.585 and 0.98 mole fraction SiO_2 and in the temperature range from 1968 K to 2240 K [16]. The possibility of a two liquids region in LiF–BeF_2 is also in agreement with findings of Thoma et al. [6], who published an experimental phase diagram of LiF–BeF_2–ZrF_4, with a miscibility gap in the BeF_2-rich corner of the ternary diagram, which nearly reaches the LiF–BeF_2 edge.

The LiF–ThF_4 diagram was measured by Thoma et al. [17], with a modification by Thoma a few years after [18]. In the earlier work, four intermediate compounds were identified by XRD, which are $3LiF\cdot ThF_4$, $7LiF\cdot 6ThF_4$, $LiF\cdot 2ThF_4$ and $LiF\cdot 4ThF_4$. The second compound has later been changed to $LiF\cdot ThF_4$. But regardless the stoichiometry, it melts congruently, the others incongruently. Gibbs energy functions are only known for the pure compounds LiF and ThF_4. The functions for the other compounds had to be assessed. This leaves evidently room for improvement of the optimization by adding further experimental data, when they become available.

The system of BeF_2–ThF_4, which was analyzed by Thoma et al. [19], is a simple eutectic system with the eutectic point very near the BeF_2 axis.

3.2. The ternary phase diagram of *LiF–BeF_2–ThF_4*

Table 3 lists the ternary eutectic and peritectic points of the calculated phase diagram of LiF–BeF_2–ThF_4, as well as the invariant points proposed by Thoma et al. [19], who investigated experimentally this ternary diagram.

Fig. 4 shows the calculated liquidus surface of LiF–BeF_2–ThF_4.

The experimental results suggest that no ternary compounds exist in the system LiF–BeF_2–ThF_4. To calculate this phase diagram, the binary Redlich–Kister coefficients could be interpolated to the ternary diagram in either a symmetric or an asymmetric way. The Muggianu or Kohler type interpolation is symmetric, while the Toop method is asymmetric. In the former, every binary interaction has an equal weight, but in the latter, selected binary interactions can be assigned a different weight. Toop interpolation is based on the fact that there is one asymmetric component in a ternary system, which is chemically different from the two other chemically similar and therefore symmetric components [20]. An example is a common anion system with two components having single valent cations and the third having a three-valent cation. The last is clearly the asymmetric component, of which the interactions are neglected.

Erroneous diagrams can result from making a wrong choice in the way of interpolation. In this study, Toop interpolation has been applied and BeF_2 has been

Table 3
Invariant equilibria in LiF–BeF_2–ThF_4, calculated and *experimental*[a]

LiF	BeF_2	ThF_4	T/K	Type invariant	Phases present
0.69	0.21	0.10	710	Eutectic	$LiF + 3LiF\cdot ThF_4 + 2LiF\cdot BeF_2 + L$
0.67	0.22	0.11	700	Eutectic	$3LiF\cdot ThF_4 + LiF\cdot ThF_4 + 2LiF\cdot BeF_2 + L$
0.49	0.46	0.05	640	Eutectic	$2LiF\cdot BeF_2 + BeF_2 + LiF\cdot ThF_4 + L$
0.37	0.52	0.11	755	Peritectic	$LiF\cdot ThF_4 + LiF\cdot 2ThF_4 + BeF_2 + L$
0.23	0.67	0.10	800	Peritectic	$LiF\cdot 2ThF_4 + LiF\cdot 4ThF_4 + BeF_2 + L$
0.66	*0.30*	*0.04*	*717*	*Peritectic*	$LiF + 3LiF\cdot ThF_4 + 2LiF\cdot BeF_2 + L$
0.63	*0.30*	*0.07*	*721*	*Peritectic*	$3LiF\cdot ThF_4 + LiF\cdot ThF_4 + 2LiF\cdot BeF_2 + L$
0.47	*0.51*	*0.02*	*629*	*Eutectic*	$2LiF\cdot BeF_2 + BeF_2 + LiF\cdot 2ThF_4 + L$
0.34	*0.64*	*0.03*	*728*	*Peritectic*	$LiF\cdot 2ThF_4 + LiF\cdot 4ThF_4 + BeF_2 + L$
0.15	*0.83*	*0.02*	*770*	*Peritectic*	$ThF_4 + LiF\cdot 4ThF_4 + BeF_2 + L$

[a] Values in *italics* are proposed values, based on experiments and extrapolation [19].

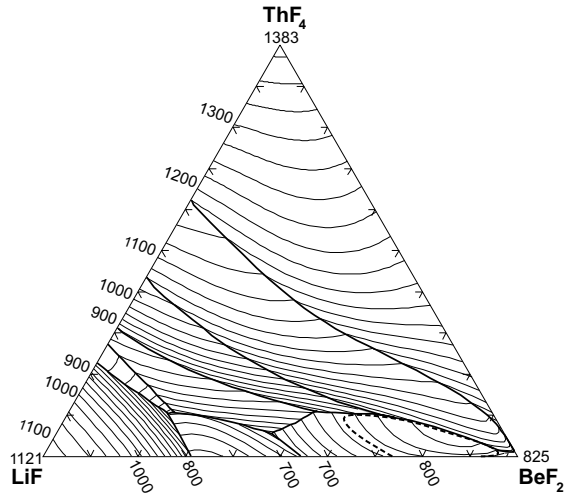

Fig. 4. The calculated liquidus surface of $LiF–BeF_2–ThF_4$. The miscibility gap is indicated as a dashed line. Isotherms are labeled in K.

selected as the asymmetric component, since it is known as a glass-former, while the other two, LiF and ThF_4, are not. Also the symmetric method has been checked, but it appeared that the resulting diagram was in poorer agreement with the experimental data compared to the asymmetric one.

The miscibility gap, which appears in the BeF_2 corner of the ternary diagram, is not directly visible in Fig. 4. This is in concordance with the method of liquidus surface plotting. Only the phase transition solid–liquid is projected, so the liquid–liquid transition in a region of demixing is ignored. But pseudobinary diagrams from BeF_2 to the opposite $LiF–ThF_4$ axis crossing the demixing area showed that the miscibility gap has an elongated oval shape, as indicated in the diagram. The height of the miscibility gap is 60 K at its maximum.

It is evident that differences exist between the experimental and the calculated diagram, imposed by the miscibility gap, which appeared in the assessment of $LiF–BeF_2$. So, especially in the BeF_2-rich edge of the diagram, the calculated phase equilibria disagree with the experimental diagram. Another aspect should be noted as well. At the time this ternary diagram was investigated experimentally, there were uncertainties whether the compound $2LiF \cdot BeF_2$ melts incongruently or not. Detailed measurements by Romberger et al. [7] revealed that it is a congruently melting compound, so that the first two invariant points by Thoma et al. could therefore be interpreted as eutectic instead of peritectic.

A comparison considering the possible composition for a Molten Salt Reactor was also made. The Molten Salt Breeder Reactor, MSBR, was designed in the 1960s to breed 233-U from 232-Th in a $LiF–BeF_2$ melt. A favorable composition was 71.7%LiF–16%BeF_2–12%ThF_4–0.3%UF_4 in moles, with the small amount of UF_4 to start the reaction [21]. The experimental temperature of fusion was determined to be 773 K, which is in agreement with the ternary phase diagram $LiF–BeF_2–ThF_4$ by Thoma et al. [19]. The composition 72%LiF–16%BeF_2–12%ThF_4 has a similar melting point, implying that the influence of the small amount of UF_4 can be neglected. The same composition has a melting point of 770 K according to the assessed ternary diagram, so experiments and thermochemical calculation are in a good agreement here.

4. Conclusion

The Molten Salt Reactor concept includes the continuous circulation of a fuel dissolved in a carrier of molten fluoride salt in order to reach high burn-up. In this paper, the system $LiF–BeF_2$ as the solvant and ThF_4 as the fertile material were considered. Thermodynamic assessments were performed for the binary sub-systems and the results were interpolated to the ternary system $LiF–BeF_2–ThF_4$. There is generally good agreement with the experimental diagrams. However, the most remarkable feature is the appearance of a miscibility gap on the BeF_2-rich side of the $LiF–BeF_2$ diagram. This caused a region of demixing in the BeF_2-rich corner of the ternary diagram as well. The assessment predicts for the MSBR composition (72%LiF–16%BeF_2–12%ThF_4) a melting point of 770 K, which agrees well with the experimental value of 773 K.

Acknowledgement

The authors thank Klaus Hack from GTT Technologies in Aachen for support in working with the FactSage software.

References

[1] E. Thilo, H.-A. Lehmann, Z. Anorg. Chem. 258 (1949) 332.
[2] J.L. Holm, O.J. Kleppa, Inorg. Chem. 8 (1969) 207.
[3] D.M. Roy, R. Roy, E.F. Osborn, J. Am. Ceram. Soc. 33 (1950) 85.
[4] D.M. Roy, R. Roy, E.F. Osborn, J. Am. Ceram. Soc. 37 (1954) 300.
[5] A.V. Novoselova, Y.P. Simanov, E.I. Jarembash, Zh. Fiz. Khim. SSSR 26 (1952) 1244.
[6] R.E. Thoma, H. Insley, H.A. Friedman, G.M. Hebert, J. Nucl. Mater. 27 (1968) 166.
[7] K.A. Romberger, J. Braunstein, R.E. Thoma, J. Phys. Chem. 76 (1972) 1154.

[8] M.W. Chase Jr. (Ed.), NIST-JANAF Thermochemical Tables, 4th Ed., J. Phys. Chem. Ref. Data Monograph, vol. 9, 1998.
[9] C.W. Bale, P. Chartrand, S.A. Degterov, G. Eriksson, K. Hack, R. BenMahfoud, J. Melançon, A.D. Pelton, S. Petersen, CALPHAD 62 (2002) 189.
[10] M. Pelikan, D.E. Goldberg, E. Cantú-Paz, in: Proceedings of the Genetic and Evolutionary Computation Conference, 1999, p. 525.
[11] H.L. Lukas, E.T. Henig, B. Zimmermann, CALPHAD 1 (1977) 225.
[12] A.D. Pelton, Thermodynamics and Phase Diagrams of Materials, vol. 5, VHC, Weinheim, 1991 (Chapter 1).
[13] C.E. Vallet, J. Braunstein, J. Am. Ceram. Soc. 60 (1977) 316.
[14] H.E. Cook, J.E. Hilliard, Trans. AIME 233 (1965) 142.
[15] B.F. Hitch, C.F. Baes Jr., Inorg. Chem. 8 (1969) 201.
[16] V.B.M. Hageman, H.A.J. Oonk, Phys. Chem. Glasses 27 (1986) 194.
[17] R.E. Thoma, H. Insley, B.S. Landau, H.A. Friedman, W.R. Grimes, J. Phys. Chem. 63 (1959) 1266.
[18] R.E. Thoma, Advances in Molten Salt Chemistry, vol. 3, Plenum, 1975, p. 275 (Chapter 6).
[19] R.E. Thoma, H. Insley, H.A. Friedman, C.F. Weaver, J. Phys. Chem. 64 (1960) 865.
[20] A.D. Pelton, Calphad 25 (2001) 319.
[21] W.R. Grimes, Nucl. Appl. Technol. 8 (1969) 137.
[22] R.J.M. Konings, J.P.M. van der Meer, E. Walle, Chemical aspects of Molten Salt Reactor fuel, Tech. Rep., 2005.